# Electronic transport properties of a two-dimensional electron gas in a silicon quantum-well structure at low temperature

A. Gold
*Physik-Department E 16, Technische Universität München, D-8046 Garching, Federal Republic of Germany*
(Received 29 April 1986)

We calculate the static and dynamic transport properties of a two-dimensional electron gas in a Si quantum well of thickness $a$ at zero temperature. Background doping, remote doping, and surface roughness are considered as the relevant scattering mechanisms. Multiple-scattering effects are included in the theory and the phase diagram for the metal-insulator transition is evaluated. Due to the anomalous wave-vector dependence of the polarizability the correction to the conductivity, which is linear in the temperature, is derived for quantum-well structures. The frequency dependence of the scattering rate is calculated. We compare our results on the mobility with recent experiments in superlattices of Si-$Si_xGe_{1-x}$ and discuss the upper limits of the mobility. For electron density $n > 10^{12}$ cm$^{-2}$ and $a > 40$ Å remote doping limits the mobility. But for $n < 10^{12}$ cm$^{-2}$ homogeneous background scattering also becomes important. Surface roughness scattering becomes dominant only for thin quantum wells with thickness smaller than 40 Å.

## I. INTRODUCTION

The study of the transport properties of a two-dimensional electron gas is a very active field in semiconductor physics. The silicon—metal-oxide semiconductor system has been studied in great detail. For a review see Ref. 1. Recently GaAs-$Al_xGa_{1-x}As$ heterostructures and quantum-well structures have also become important. In this system the ionized donors are separated from the two-dimensional electron gas, and so these structures have a high mobility. For a review see Ref. 2. Very new are structures of Si-$Si_xGe_{1-x}$ strained layers, realized as superlattices, quantum-well structures, and heterostructures.[3–5] For a recent review on Si-$Si_xGe_{1-x}$ superlattices see Ref. 6. It was found in Si-$Si_xGe_{1-x}$ superlattices that a two-dimensional electron gas is formed and it was suggested that the carriers are confined in the silicon layers.[3] Recent calculations of the subband structure[7] support this idea. The Si-$Si_xGe_{1-x}$ superlattices have been doped with a method denoted as secondary implantation.[8] The mobility for low temperatures depends strongly on the position of the dopant layer, and a weaker dependence was reported for room temperature.[6]

Transport theory for quantum-well structures[9–11] follows the theoretical work of Stern and Howard[12] for inversion layers. In the work of Ref. 9 the finite extension of the quantum well, which gives rise to some form factors for the electron impurity and the electron-electron interaction, has been neglected. This effect has been taken into account in Refs. 10 and 11 for homogeneous doping in the quantum well and homogeneous doping on the right side of the quantum well.

We discuss in this paper the scattering from a two-dimensional sheet of impurities (remote doping) and from a homogeneously doped three-dimensional structure (homogeneous background doping). Due to differences of the models, a direct comparison of our work with the work of Refs. 10 and 11 is not possible. Moreover, it is not clear from Ref. 10 how the $z$ dependence of the potentials (Eqs. 7 and 8 of Ref. 10) is eliminated in the final results for the mobility. Local-field effects reduce the screening properties of the interacting electron gas and decrease the mobility for a given random potential. This was discussed for metal-oxide—semiconductor systems in Refs. 13 and 14. In the case of quantum wells this effect is discussed for the first time in this paper.

For surface-roughness scattering the theory of Ref. 9 is inconsistent, because the finite quantum-well width is taken into account for the surface-electron interaction, but for the screening a zero quantum-well width was assumed. In this paper a finite quantum well is also assumed for the screening behavior, besides the new effects due to local-field corrections.

The theory of Ref. 12 cannot account for multiple-scattering effects. In this paper we extend our transport theory, which includes multiple-scattering effects and a description of the metal-insulator transition[13,14] to quantum-well structures and various scattering mechanisms. Parameters for Si-$Si_xGe_{1-x}$ are used. For remote impurity doping, homogeneous background doping and surface-roughness scattering, we will discuss the upper limits for the mobility at zero temperature. Due to multiple-scattering effects, a transition to an insulator is expected for low electron density. We predict the phase diagram for the metal-insulator transition. The behavior of the momentum relaxation time for low temperatures is evaluated by following the work of Ref. 15. The dynamic conductivity for homogeneous doping is calculated and plasmon anomalies are predicted.

The paper is organized as follows. In Sec. II we explain the model and the transport theory. The mobility for the various scattering mechanisms is discussed in Sec. III. Some aspects of the dynamical conductivity are evaluated in Sec. IV. In Sec. V we compare our theoretical results

 

with experimental results of Ref. 6 and propose some experiments. A conclusion of the paper is given in Sec. VI and some quantum-well structures are designed there in order to test some of the predictions of this paper.

## II. MODEL AND THEORY

In this part of the paper we specify the system under consideration and the transport theory.

### A. Scattering mechanisms

We evaluate the conductivity of a two-dimensional electron gas in a quantum-well structure. The subband structure is neglected and only the lowest subband is included in the calculation. We assume that the electrons can move in the $xy$ plane and are confined in the $z$ plane. The wave function $\psi(z)$ for the $z$ direction is given by the quantum-well width $a$ via

$$\psi(z)=\left[\frac{2}{a}\right]^{1/2}\sin\left[\frac{\pi z}{a}\right],\quad 0\le z\le a \tag{1}$$

and is zero for all other $z$, see Fig. 1.

We assume that a two-dimensional sheet of donors with a two-dimensional density $n_i$ can be implanted in the system at a distance $z_i$ from the boundary of the quantum well, see Fig. 1. The random potential $U_1(q)$ for wave number $q$ is expressed as

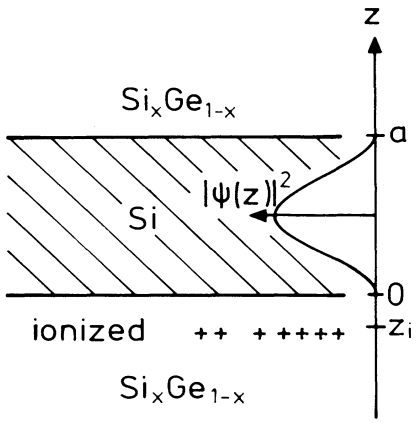


FIG. 1. Configuration of the single quantum well. $\psi(z)$ is given by Eq. (1).

$$\langle\,|\,U_1(q)\,|^2\rangle=n_i\left[\frac{2\pi e^2}{\epsilon_L}\frac{1}{q}\right]^2 F_R(q,z_i)^2\,, \tag{2a}$$

with

$$F_R(q,z_i)=\int_{-\infty}^{\infty}dz\;|\,\psi(z)\,|^2 e^{-q\,|z-z_i|}\,. \tag{2b}$$

Explicitly we find

$$F_R(q,z_i)=\frac{8\pi^2}{aq}\frac{1}{4\pi^2+a^2q^2}\begin{cases}\frac{1}{2}e^{qz_i}(1-e^{-qa}) & z_i<0\\ 1-\frac{1}{2}e^{-qz_i}-\frac{1}{2}e^{-q(a-z_i)}+\dfrac{q^2a^2}{2\pi^2}\sin^2\left[\dfrac{\pi z_i}{a}\right], & 0\le z_i\le a\\ \frac{1}{2}e^{-q(z_i-a)}(1-e^{-qa}) & z_i>a\,.\end{cases} \tag{2c}$$

$\epsilon_L$ is the dielectric constant of the host lattice and $F_R(q,z_i)$ accounts for the distance $z_i$ between the impurity layer and the quantum well and for the finite width of the quantum well.[1] In the following we will refer to this scattering mechanism as remote doping. Especially, we will discuss this scattering mechanism for $z_i=-a/2$ and $z_i=a/2$.

The second scattering mechanism for which we account is due to homogeneous background doping of the volume characterized by the three-dimensional density $N_B$. The random potential is written as

$$\langle\,|\,U_2(q)\,|^2\rangle=N_B a\left[\frac{2\pi e^2}{\epsilon_L}\frac{1}{q}\right]^2 F_B(q)\,, \tag{3a}$$

with

$$F_B(q)=\frac{1}{a}\int_{-\infty}^{\infty}dz_i F(q,z_i)^2\,. \tag{3b}$$

Explicitly, we get

$$F_B(q)=\frac{1}{aq}\left[\frac{4\pi^2}{4\pi^2+a^2q^2}\right]^2\left\{\frac{4}{q^2a^2}\left[1-\frac{7}{4}\frac{1}{qa}-\frac{1}{4}\frac{1}{qa}e^{-2qa}+\left[\frac{2}{qa}+\frac{1}{2}\right]e^{-qa}\right]\right.$$
$$\left.+\left[\frac{1-e^{-qa}}{aq}\right]^2+4\left[\frac{3}{32}\frac{q^2a^2}{\pi^2}+\frac{1}{2\pi^2}-\frac{1}{qa}\frac{1-e^{-aq}}{4\pi^2+a^2q^2}\right]\right\}. \tag{3c}$$

$F_B(q)$ accounts for the finite quantum well and the homogeneous distribution of the Coulomb-like impurities in the volume of the structure.

The third scattering mechanism which we consider is surface-roughness scattering according to the ideas of Prange and Nee.[16] The roughness at the quantum-well boundary is characterized by the height $\Delta$ and the length $\Lambda$ of the Gaussian-like fluctuations. We assume that roughness at $z=0$ and $z=a$ can be characterized by the same parameters and that there is no interference between the two interfaces. The random potential is then expressed as

$$\langle | U_3(q) |^2 \rangle = 2 \left[ \frac{4\pi}{a^2} \right] \left[ \frac{m^*}{m_z} \right]^2 \left[ \frac{\pi}{k_F a} \right]^4 (\varepsilon_F \Delta \Lambda)^2 e^{-q^2\Lambda^2/4} . \tag{4}$$

The factor 2 on the right-hand side of Eq. (4) comes from the two interfaces and $\varepsilon_F$ is the Fermi energy and $k_F$ the Fermi wave number of the two-dimensional electron gas. $m_z$ is the mass perpendicular to the interface. According to Eq. (4), $\langle | U_3(q) |^2 \rangle \propto 1/a^6$ and for very thin quantum wells the surface-roughness scattering should dominate all other scattering mechanisms. Quantum wells with small $a$ should be useful to study the roughness of the quantum-well interface.

The electron-electron interaction $V(q)$ of the electrons in the quantum well is characterized by a Coulomb potential and a form factor due to finite confinement[1] and is given by

$$V(q) = \frac{2\pi e^2}{\epsilon_L} \frac{1}{q} F_C(q) , \tag{5a}$$

with

$$F_C(q) = \int_{-\infty}^{\infty} dz \, | \psi(z) |^2 \int_{-\infty}^{\infty} dz' \, | \psi(z') |^2 e^{-q|z-z'|} . \tag{5b}$$

Explicitly we evaluate

$$F_C(q) = \frac{1}{4\pi^2 + a^2q^2} \left[ 3aq + \frac{8\pi^2}{aq} - \frac{32\pi^4}{a^2q^2} \frac{1-e^{-aq}}{4\pi^2 + a^2q^2} \right] . \tag{5c}$$

$F_R(q,z_i)$ and $F_C(q)$ are shown in Fig. 2 as a function of $q$. Later it is shown that the $q \to 0$ behavior of the random potential and the electron-electron interaction determines various properties of the system. We find

$$\langle | U_i(q) |^2 \rangle \propto q^{\alpha} , \tag{6}$$

and $\alpha = -2$ for remote doping, $\alpha = -3$ for homogeneous background doping, and $\alpha = 0$ for surface-roughness scattering. For $F_C(q)$ we find

$$F_C(q \to 0) = 1 - \left[ \frac{1}{3} - \frac{5}{4\pi^2} \right] aq . \tag{7}$$

In the following we will evaluate the transport properties of the quantum well for $Si_xGe_{1-x}$-Si-$Si_xGe_{1-x}$. The dielectric constant is given as $\epsilon_L = 11.5 + 2.25(1-x)$ and

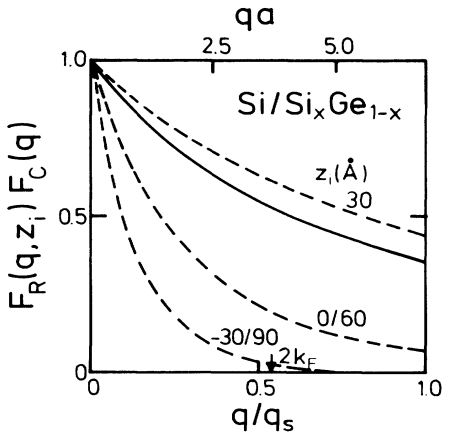


FIG 2. Form factors $F_R(q,z_i)$ (dashed lines) and $F_c(q)$ (solid line) versus $q$. The arrow indicates $2k_F$ for $n = 3 \times 10^{12}$ cm$^{-2}$. $a = 60$ Å.

we assume $x = 0.5$ and then $\epsilon_L = 12.6$. The two-dimensional electron gas is assumed to be confined in the silicon layer with the transport mass $m^* = 0.19 m_e$ and $m_z = 0.916 m_e$. $m_e$ is the vacuum mass of the electron. The valley degeneracy $g_v$ is assumed to be 2. The relation between the electron density $n$ and the Fermi wave number is given by $n = (g_v/2\pi) k_F^2$. $\epsilon_L$ and $m^*$ determine the effective Bohr radius $a^*$ via the hydrogen Bohr radius $a_H$ as $a^* = a_H \epsilon_L m_e / m^*$. The screening wave number $q_s$ is given by $q_s = 2g_v/a^*$. We put $\hbar = 1$ in this paper.

### B. Transport theory

According to the random potentials the momentum relaxation time $\tau$ for the electrons in the quantum well is finite. Within the Howard-Stern formulation[12] we can write

$$\frac{1}{\tau} = \frac{1}{2\pi\epsilon_F} \int_0^{2k_F} dq \frac{q^2}{(4k_F^2 - q^2)^{1/2}} \frac{\langle | U(q) |^2 \rangle}{\epsilon(q)^2} . \tag{8}$$

$\epsilon(q)$ is the dielectric function of the two-dimensional electron gas and we use[13,14]

$$\epsilon(q) = 1 + V(q)[1 - G(q)] X^0(q) . \tag{9}$$

$X^0(q)$ is the polarizability of the two-dimensional electron gas[17] and $G(q)$ is the Hubbard form of the local-field correction.[18] For $G(q) = 0$, $X^0(q) = X^0$ $(q = 0)$, and $F_c(q) = 1$, one gets the Thomas Fermi result for dimension two: $\varepsilon(q) = 1 + q_s/q$. The mobility $\mu$ is connected with $\tau$ via $\mu = (e/m^*)\tau$ and the static conductivity $\sigma$ is given by $\sigma = ne\mu$.

The dynamic conductivity is written as[19]

$$\sigma'(\omega) = \frac{ne^2}{m^*} \frac{M''(\omega)}{[\omega + M'(\omega)]^2 + M''(\omega)^2} \tag{10}$$

and $M'(\omega)$ is the real part and $M''(\omega)$ the imaginary part of the current relaxation kernel. Equation (9) generalizes the Drude result by a finite $M'(\omega)$ and a frequency dependence of the relaxation time.

According to the theory of Ref. 13 we take into account multiple-scattering effects and $M'^{(\prime\prime)}(\omega)$ is given as

$$M'^{(\prime\prime)}(\omega)=\frac{1}{4\pi nm^*}\int_0^\infty dq\, q^3\langle\,|\,U(q)\,|^2\rangle\phi'^{(\prime\prime)}(q,\omega)\ . \tag{11}$$

$\phi'^{(\prime\prime)}(q,\omega)$ is the real (imaginary) part of the density correlation function of the interacting electron gas. The interaction is treated in random-phase approximation including local-field corrections. $\phi'^{(\prime\prime)}(q,\omega)$ depends on $M'(\omega)$ and $M''(\omega)$ and details of the theory can be found in Ref. 13. If multiple-scattering effects are neglected, then $\phi''(\omega)$ is proportional to the random-phase approximation for the density relaxation function (Lindhard function). $M''\ (\omega=0)$ is then given by $1/\tau$ from Eq. (8).

Equation (11) describes the decay of the current modes into the density modes of the interacting electron gas. Within the random-phase approximation we consider, as the relevant density modes, particle-hole excitation and plasmons. An equation equivalent to Eq. (11) has been written down in Ref. 20, but self-consistent effects have not been taken into account. Recently it has been claimed in Ref. 21 that in Ref. 20 the plasmon decay channel has been ignored. But it has been shown in Refs. 13, 14, and 22 that this plasmon channel is very important and that the plasmon anomalies already have been found in experiments,[23] for a review see Ref. 24.

Due to the anomalous $q$ dependence of the polarizability, the conductivity shows an anomalous temperature behavior at low temperature.[25] At low temperature $T$ the conductivity can be written as[15]

$$\sigma(T)=\sigma(T=0)\left[1-C(\alpha,n)\frac{T}{\varepsilon_F}-O(T^{3/2})\right]\ , \tag{12a}$$

with

$$C(\alpha,n)=\frac{\varepsilon_F}{T}\frac{\tau}{\Delta\tau}\ . \tag{12b}$$

$\alpha$ describes the $q$ dependence of the random potential for $q\to 0$, see Eq. (6). $\Delta\tau$ gives the temperature-dependent part of the momentum relaxation time and analytic expressions for $\tau$ and $\Delta\tau$ were given in Ref. 15. Here we use the analytical expression for $\Delta\tau$ but use Eq. (8) for $\tau$. A linear $T$ dependence was found in experiments[26–28] on silicon metal oxide semiconductor systems with high mobility. So one could expect such a temperature behavior for silicon quantum wells, too. Explicit results are given in the next chapter.

## III. STATIC CONDUCTIVITY

In the first part of this chapter I discuss the upper limits of the mobility for the three scattering mechanisms. In the second part I describe the metal-insulator transition and the low-temperature corrections.

### A. Background impurity doping

The mobility $\mu_B$ for background doping is given by Eqs. (3) and (8). Due to the $q=2k_F$ singularity in Eq. (8) we can evaluate the $q$ integral in an approximation where the square-root singularity at $q\approx 2k_F$ is integrated, but the form factors are taken at $q=2k_F$. This approximation works very well at low electron densities and gives the correct trend for higher electron densities. We receive for background doping

$$\frac{1}{\tau}=\frac{\pi}{g_v}\varepsilon_F\frac{N_B a}{n}\frac{F_B(2k_F)}{\{[1-G(2k_F)]F_C(2k_F)+2k_F/q_s\}^2}\ . \tag{13a}$$

For $2k_F a\ll 1$ we find $F_B(2k_F)=1/(2k_F a)$. From Eq. (13a) for $2k_F/q_s\ll 1$ we get a $\mu\propto n^{1/2}$ behavior

$$\mu=2e\frac{g_v^2}{\pi^2}\frac{k_F}{N_B}[1-G(2k_F)]^2\ , \tag{13b}$$

and for $2k_F/q_s\gg 1$ we obtain

$$\frac{1}{\tau}=\frac{\pi}{g_v}\varepsilon_F\frac{N_B a}{n}\frac{F_B(2k_F)}{(2k_F/q_s)^2}\ , \tag{13c}$$

which corresponds to a $\mu\propto n^{3/2}$ behavior for high densities. The transition from the $\mu\propto n^{1/2}$ to the $\mu\propto n^{3/2}$ behavior should occur at $n=q_s^2/(4\pi)\approx 1\times 10^{13}\ \mathrm{cm}^{-2}$.

In Fig. 3 we give our numerical results according to Eqs. (3) and (8). For low densities $\mu_B$ is independent of $a$, see Eq. (13b). Local-field corrections decrease the screening properties of the electron gas and the mobility is lower if local-field corrections are taken into account. For higher densities there is an $a$ dependence in Fig. 3 which indicates that already higher-order terms than $F_B(2k_F)=1/(2k_F a)$ play a role. We expect that at least at low electron densities the background doping could limit the mobility.

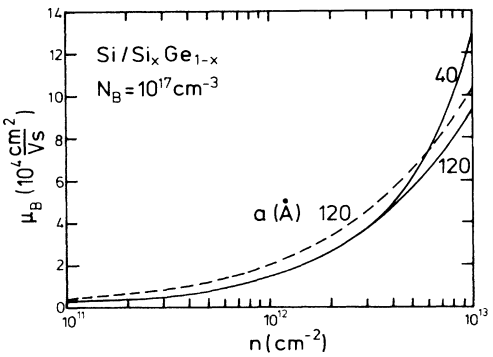


FIG. 3. Mobility due to homogeneous background doping according to Eqs. (3) and (8) versus density, as solid lines. The dashed line is for $G=0$.

### B. Remote impurity doping

According to Ref. 15 we find with Eqs. (2) and (8) the approximation for $1/\tau$ in the form

$$\frac{1}{\tau}=\varepsilon_F\frac{\pi}{g_v}\frac{n_i}{n}\frac{F_R(2k_F,z_i)^2}{\{[1-G(2k_F)]F_C(2k_F)+2k_F/q_s\}^2} . \quad (14a)$$

For low density $F_R=F_C=1$ and $\mu_R\propto 1/n$ for $n_i=n$. For higher electron density $F_F^2(2k_F,z_i=-a/2)=e^{-k_Fa}$ and a strong dependence of the mobility on the quantum-well width is expected. Numerical results are shown in Fig. 4 for $z_i=-a/2$. With $\mu_R\propto e^{k_Fa}/n$ we see that at high density the factor $e^{k_Fa}$ increases the mobility and dominates over the factor $1/n$. The minimum in the $\mu_R$ versus $n$ curves is expected at $n=g_v/(2\pi a^2)$. For $a=60$ Å the minimum mobility is $9\times10^3$ cm$^2$/Vs at $n=5\times10^{11}$ cm$^{-2}$.

In Fig. 5 the mobility $\mu_R$ versus density is shown for $z_i=a/2$ according to Eqs. (2) and (8). The form factor, which goes into Eq. (14), is given by

$$F_R\left[2k_F,z_i=\frac{a}{2}\right]=\frac{\pi^2}{ak_F}\frac{1}{\pi^2+a^2k_F^2}\left[1-e^{-ak_F}+\left[\frac{ak_F}{\pi}\right]^2\right] . \quad (14b)$$

For low density with $F_R(2k_F)=1$ and $n_i=n$ the mobility increases with decreasing density: $\mu_R\propto 1/n$. For high electron density with $2k_F/q_s\gg F_C(2k_F)$ the mobility follows the law $\mu_R\propto 1/F_R(2k_F,z_i=a/2)^2$. With increasing density $F_R(2k_F)$ decreases and $\mu_R$ increases, see Fig. 2. $F_R(2k_F)$ depends on $a$, see Eq. (14b), and the density for the minimum mobility also depends on $a$. For low density the mobility does not depend on $a$,

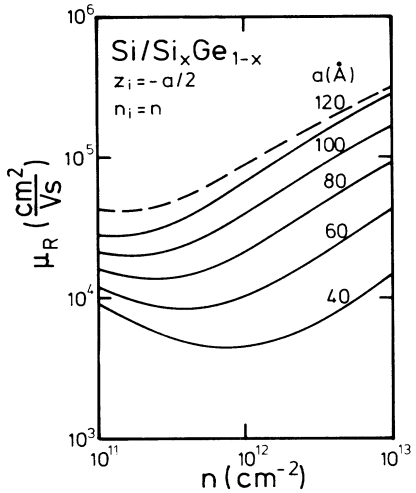


FIG. 4. Mobility due to remote doping according to Eqs. (2) and (8) versus density, as solid lines for $z_i=-a/2$. The dashed line is for $G=0$ and $a=120$ Å.

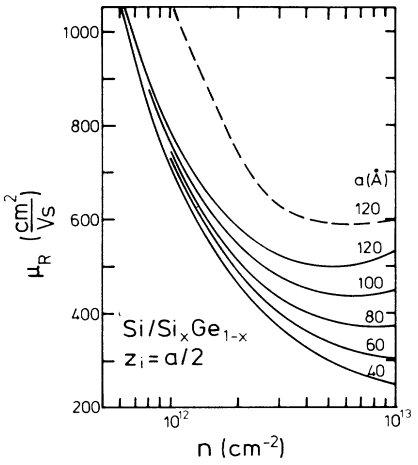


FIG. 5. Mobility due to remote doping according to Eqs. (2) and (8) versus density, as solid lines for $z_i=a/2$. The dashed line is for $G=0$.

$$\mu=\frac{e}{m^*}\frac{g_v}{\pi}\frac{1}{\varepsilon_F}\frac{n}{n_i}[1-G(2k_F)]^2 , \quad (14c)$$

and finite local-field corrections decrease the mobility. This effect has also been discussed for metal-oxide silicon semiconductors.[13]

### C. Surface-roughness scattering

With Eqs. (4) and (8) we can evaluate the mobility $\mu_S$ due to surface-roughness scattering in an approximation which has been discussed before.[15] For $k_F\Lambda\ll 1$ we get

$$\frac{1}{\tau}=\varepsilon_F 12\pi^5\left[\frac{\Delta^2\Lambda^2}{a^6q_s^2}\right]\left[\frac{m^*}{m_z}\right]^2\times\frac{1}{\{[1-G(2k_F)]F_C(2k_F)+2k_F/q_s\}^2} , \quad (15a)$$

and for $k_F\to 0$ we find

$$\mu=\frac{e}{m^*}\left[\frac{m_z}{m^*}\right]^2\frac{a^6q_s^2}{\Delta^2\Lambda^2}\frac{1}{12\pi^5}\frac{1}{\varepsilon_F}[1-G(2k_F)]^2 . \quad (15b)$$

For low electron concentration we find $\mu\propto 1/n$. In the case $k_F\Lambda\gg 1$, we get

$$\frac{1}{\tau}=\varepsilon_F 24\pi^{9/2}\frac{\Delta^2}{\Lambda^3a^6k_F^5q_s^2}\left[\frac{m^*}{m_z}\right]^2\times\frac{1}{\{[1-G(2/\Lambda)]F_C(2/\Lambda)+2/\Lambda q_s\}^2} \quad (16)$$

and $\mu\propto n^{3/2}$. The crossover of the $\mu\propto 1/n$ to the long-range (LR) $\mu\propto n^{3/2}$ behavior is at $n=n_{\rm LR}=g_v/(2\pi\Lambda^2)$.

Due to the factor $(m^*/m_z)^2$ in Eq. (4) surface-roughness scattering is strongly suppressed for silicon quantum wells. In a GaAs quantum well with $m^*/m_z=1$ surface-roughness scattering is more important.

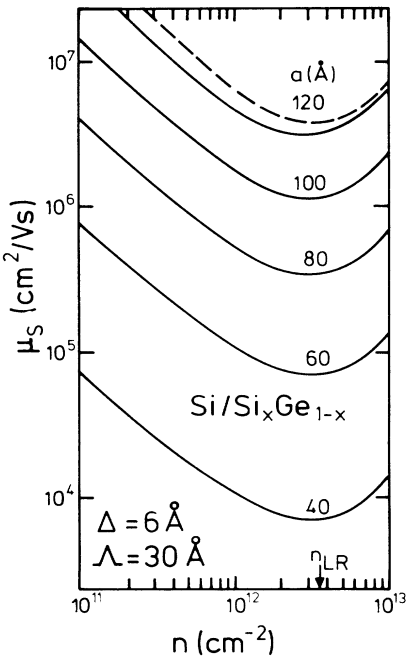


FIG. 6. Mobility due to surface-roughness scattering according to Eqs. (4) and (8) versus density, as solid lines. The dashed curve is for $G=0$ and $a=120$ Å. $n_{LR}$ is defined as $n_{LR}=1/(2\pi\Lambda^2)$.

In Fig. 6 we show our numerical results for $\mu_S$ versus density. Again the local-field effects decrease the mobility, see Eq. (15b). At low densities with $F_c(q)=1$ one gets $\mu \propto a^6$. So we find that for thin quantum wells ($a<40$ Å) the surface-roughness scattering becomes very important, while for thick quantum wells ($a>40$ Å) the surface-roughness scattering is dominated by homogeneous background doping or remote doping. Naively one would argue that an increasing $\Lambda$ corresponds to a smoother interface. But for $k_F\Lambda \ll 1$, $\mu \propto 1/\Lambda^2$. Only for $k_F\Lambda \gg 1$ does one find that $\mu$ increases with increasing $\Lambda$ or increasing smoothness of the interface.[14]

### D. Metal-insulator transition

It has been found in Ref. 13 that multiple-scattering effects in the case of charged impurity scattering lead at low electron density to a phase which is characterized by a zero dc conductivity and a finite dc polarizability. Experiments[29] done on metal-oxide–silicon semiconductor systems are in good agreement with the theory.[13] The phase-transition line is given by $A=1$ (Ref. 30) and $A$ is written as[13]

$$A=\frac{1}{4\pi n^2}\int_0^\infty dq\, q\frac{\langle\,|U(q)|^2\rangle}{\epsilon(q)^2}X^0(q)^2\ . \tag{17a}$$

If more than one scattering mechanism is considered and if correlations between the various scattering mechanisms are neglected, we must use for our three scattering mechanisms the form

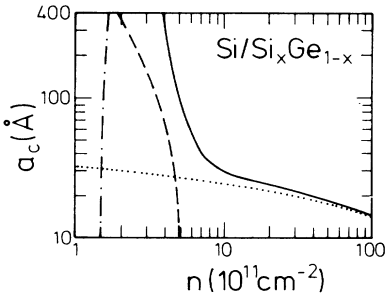


FIG. 7. Critical quantum-well thickness $a_c$ versus density according to Eq. (17a) and $A=1$. For $a<a_c$ the dc conductivity is zero, while for $a>a_c$ the dc conductivity is finite. The dotted, dashed-dotted, and dashed lines are surface roughness, background doping, and remote doping, respectively. The solid line is for the three scattering mechanisms. The parameters are $n=n_i$, $z_i=a_c/2$, $N_B=10^{17}$ cm$^{-2}$, $\Delta=6$ Å, and $\Lambda=30$ Å.

$$\langle\,|U(q)|^2\rangle=\sum_{i=1}^{3}\langle\,|U_i(q)|^2\rangle\ . \tag{17b}$$

In Fig. 7 we show the critical quantum-well thickness $a_c$, where $A=1$, versus density. For $a>a_c$ the system shows metallic conductivity and for $a<a_c$ the dc conductivity is zero. The dashed line is for remote doping with $z_i=a/2$. The solid line is for the three scattering mechanisms.

At high electron density the insulator phase for the three scattering mechanisms is strongly increased in comparison to remote doping (dashed line). This comes from the fact that for small $a$ the surface-roughness scattering dominates all other scattering mechanisms because of $\langle\,|U_3(q)|^2\rangle \propto (\Delta\Lambda)^2/a^6$. So at high electron concentration we find localization due to surface-roughness scattering. At low electron concentration the insulator phase is increased in comparison to remote doping due to surface-roughness scattering and the homogeneous background doping. We mention that $a_c$ for high electron density depends on the parameters of the surface-roughness scattering. But the dependence is only a weak one; for example, $a_c \propto (\Delta\Lambda)^{1/3}$ for $k_F\Lambda \ll 1$.

### E. Low-temperature corrections

The coefficient $C(\alpha,n)$ determines the temperature dependence of the conductivity at low temperatures, see Eq. (12). In the work of Gold and Dolgopolov[15] $C(\alpha,n)$ was given analytically via Eq. (12b) and analytical expressions for $\tau$ and $\Delta\tau$. A more accurate expression for $C(\alpha,n)$ is obtained if $\tau$ is calculated according to Eq. (8) and

$$\frac{1}{\Delta\tau}=2T\ln 2k_F^2\frac{\langle\,|U(2k_F)|^2\rangle}{\epsilon_F^2}\times\frac{V(2k_F)\rho_F[1-G(2k_F)]}{\{1+V(2k_F)\rho_F[1-G(2k_F)]\}^3} \tag{18}$$

from Ref. 15 is used.

Explicitly we find for homogeneous background

scattering ($\alpha=-3$),

$$C(-3,n)=\varepsilon_F\tau\frac{4\pi}{g_v}\ln 2\frac{N_B a}{n}F_B(2k_F)\tilde{C}(n)\ , \tag{19a}$$

for remote impurity scattering ($\alpha=-2$),

$$C(-2,n)=\varepsilon_F\tau\frac{4\pi}{g_v}\ln 2\frac{n_i}{n}F_R(2k_F,z_i)^2\tilde{C}(n)\ , \tag{19b}$$

and for surface-roughness scattering ($\alpha=0$),

$$C(0,n)=\varepsilon_F\tau 32\pi^5\ln 2\left[\frac{m^*}{m_z}\right]^2\left[\frac{\Delta\Lambda}{a^3q_s}\right]^2 e^{-k_F^2\Lambda^2}\tilde{C}(n)\ . \tag{19c}$$

The density dependent parameter $\tilde{C}(n)$ is given by

$$\tilde{C}(n)=\frac{F_C(2k_F)[1-G(2k_F)]}{\{[1-G(2k_F)]F_C(2k_F)+2k_F/q_s\}^3}\ . \tag{19d}$$

$C(\alpha,n)$ versus density is shown in Fig. 8 for the three scattering mechanisms. $C(-2,n)$ decays to zero for increasing density very rapidly because of $F_R(2k_F)$, see Fig. 2. An experimental finding of a variation of the conductivity linear in temperature could be used to verify the form factors $F_C(q)$, $F_B(q)$, and $F_R(q)$ and could give information on $G(2k_F)$.

In experiment always all scattering mechanisms contribute to the resistance and to the temperature dependence. For our three scattering mechanisms we find

$$\sigma(T)=\sigma_0(T=0)\left[1-C_3(n)\frac{T}{\varepsilon_F}+O(T^{3/2})\right]\ , \tag{20a}$$

with

$$\sigma_0(T=0)=\frac{ne^2}{m^*}\frac{\tau_1\tau_2\tau_3}{(\tau_2\tau_3+\tau_1\tau_3+\tau_1\tau_2)} \tag{20b}$$

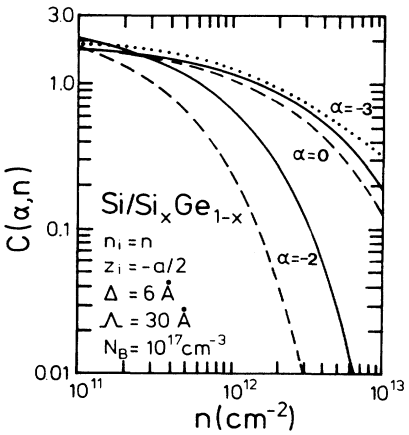


FIG. 8. Parameter $C(\alpha,n)$ versus density for different scattering mechanisms according to Eq. (19). The solid lines and the dotted line are for $a=60$ Å. The dashed lines are for $a=100$ Å.

and with $C_i=C(\alpha_i,n)$

$$C_3(n)=\frac{C_1\tau_2\tau_3+C_2\tau_1\tau_3+C_3\tau_1\tau_2}{\tau_2\tau_3+\tau_1\tau_3+\tau_1\tau_2}\ . \tag{20c}$$

It is easy to show that

$$\min(C_1,C_2,C_3)<C_3(n)<\max(C_1,C_2,C_3)\ . \tag{21}$$

An example will be discussed in Sec. V.

## IV. DYNAMICAL CONDUCTIVITY

In this section we discuss the dynamical transport properties of the quantum well. Because experimental work has not been done until now, we discuss some results which are interesting from a theoretical point of view and give some hints for the parameter regime where dynamical anomalies could be found in experiments.

### A. Non-Drude behavior

It has already been pointed out that the current can decay by exciting plasmons and particle-hole pairs, if there is some disorder in the system. For charged impurities this was discussed in Refs. 13, 22, 23, and 31. Recently this phenomenon has been rediscovered in Ref. 21. For surface-roughness scattering this effect has been discussed in Ref. 14. The decay of the current into plasmons increases the imaginary part of the current relaxation function $M''(\omega)$ in some frequency range and according to Eq. (10) we get for $\omega\gg|M'|,M''$

$$\sigma'=\frac{ne^2}{m^*}\frac{M''(\omega)}{\omega^2}\ , \tag{22a}$$

an increase of the conductivity in comparison to the Drude result:

$$\sigma'_D=\frac{ne^2}{m^*}\frac{M''(\omega=0)}{\omega^2}\ . \tag{22b}$$

The plasmon contribution to $M_p''(\omega)$ can be calculated analytically for $\omega\to 0$.[13] The frequency dependence depends only on the $q\to 0$ behavior of the random potential[14] and may be expressed as [see Eq. (6)]

$$M_p''(\omega)=K(\alpha)\varepsilon_F\left[\frac{\omega}{\varepsilon_F}\right]^{9+2\alpha}\ . \tag{23a}$$

For homogeneous background doping we get the new result

$$K(-3)=\frac{\pi}{8}\frac{1}{g_v^2}\left[\frac{N_B a^*}{n}\right]\ , \tag{23b}$$

and for surface-roughness scattering we receive the new prefactor

$$K(0)=\frac{\pi^4}{2^9}\frac{1}{g_v^6}\frac{\Delta^2\Lambda^2(a^*)^6k_F^4}{a^6}\left[\frac{m^*}{m_z}\right]^2\ . \tag{23c}$$

In Fig. 9 we show $M''(\omega)$ and $\sigma'(\omega)$ for homogeneous background doping. The dashed line is according to Eq. (23). The non-Drude behavior is the difference between

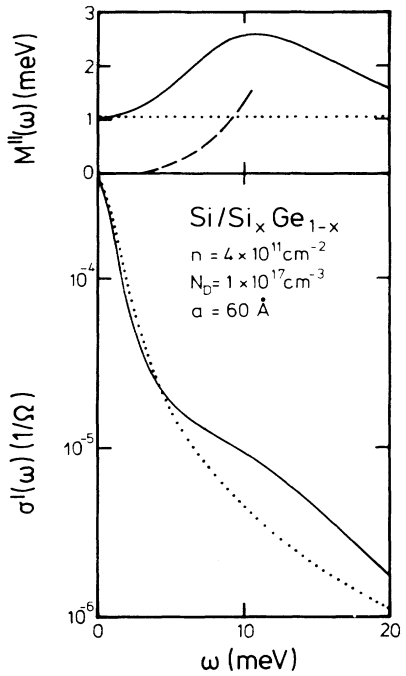


FIG. 9. $M''$ and $\sigma'$ versus frequency for homogeneous background scattering according to our self-consistent theory, as solid lines. The dotted lines represent the Drude result. The dashed line is according to Eq. (23).

the solid and dotted line. Because of the $f$-sum rule the conductivity at low frequency is lower than in the Drude theory. The crossover frequency in Fig. 9 is at 4 meV. With a higher $N_B$ value, as in Fig. 9, the dc conductivity would be lower and the high-frequency conductivity would be higher than in Fig. 9, and then the effect should be measurable in experiments analogous to the experiments done in silicon metal-oxide—semiconductor systems.[23]

### B. Linewidth of plasmons

The plasmon dispersion for a two-dimensional electron gas is for $q \to 0$ given by[17]

$$\omega_{p0} = \left[ \frac{2\pi n e^2}{m \epsilon_L} q \right]^{1/2} . \tag{24}$$

Because of the quantum-well structure, because of local-field corrections,[18] and because of additional $q$-dependent terms in a hydrodynamic expansion[17] the plasmon energy is written in the case of a quantum well as

$$\omega_p = \omega_{p0} \left[ 1 - \tfrac{1}{2}[F_C(q \to 0) - 1] - \frac{1}{4 g_v} \frac{q}{k_F} + \frac{3}{4} \frac{q}{q_s} + O(q^2) \right] , \tag{25}$$

where $F_C(q \to 0) - 1 = [\frac{1}{3} - (5/4\pi^2)]aq$, see Eq. (7).

Plasmons in quantum wells have been studied recently.[32] The varying of the parameter $a$ (and so $F_C$) seems to be an appropriate tool to study the nonlocality of the plasmon dispersion.[33]

Due to disorder the plasmons have a finite linewidth.[34] This effect has been studied carefully in metal-oxide—silicon semiconductor systems, for a review see Ref. 35. It has been shown by Gold and Götze[13] that disorder shifts the plasmon energy $\Omega$ to

$$\Omega = \omega_p - M'(\omega_p) , \tag{26a}$$

and the linewidth $\Gamma$ is given by

$$\Gamma = M''(\omega_p) . \tag{26b}$$

Within this theory the relevant experiments[34,35] have been explained.[14]

In Fig. 10 we show $M''$ as function of the density for $\omega = 0$, 5, and 10 meV. From this Fig. 10 we conclude that at high electron densities ($n > 10^{12}$ cm$^{-2}$, $\omega_{p0} < 10$ meV) $\Gamma$ in Eq. (26b) is given by the static value $M''(0)$. For $n < 10^{12}$ cm$^{-2}$ deviations of the linewidth from the static transport value $1/\tau$ may be found in experiments. The strong increase of $M''$ ($\omega = 0$) for low densities in Fig. 10 is due to multiple-scattering effects and signals the metal-insulator transition.

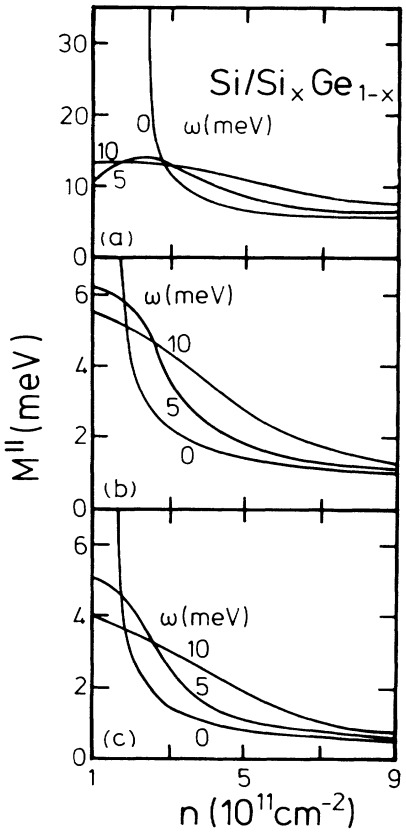


FIG. 10. $M''(\omega)$ versus density for various frequencies according to our self-consistent theory. (a) Surface-roughness scattering ($a = 30$ Å, $\Delta = 6$ Å, $\Lambda = 30$ Å). (b) Remote doping ($a = 60$ Å, $n_i = 10^{11}$ cm$^{-2}$, $z_i = a/2$). (c) Homogeneous background doping ($a = 60$ Å, $N_B = 10^{17}$ cm$^{-3}$).

In Fig. 10(a) a metal-insulator transition due to surface-roughness scattering for $a = 30$ Å is shown. This figure demonstrates the importance of surface-roughness scattering for the transport processes in quantum wells with $a < 40$ Å. A systematic study of the mobility of samples with different thickness could easily verify this effect.

The shift of the plasmon resonance due to $M'$ will not be discussed here, because experiments are not yet available. But a shift to lower frequency because of a positive $M'$, see Eq. (26a), is expected. This was also found in silicon metal-oxide–semiconductor systems, for a review see Ref. 35.

## V. MULTILAYER SYSTEM

In this chapter we compare our theoretical results with experiments in Si-$Si_xGe_{1-x}$ strained layer superlattices. Two models will be considered. The interaction between the layers of the superlattice is ignored.

### A. Model I: $n_i = n$ for remote doping

In the experiment of Ref. 3 a superlattice was used and the mobility of one layer was plotted versus the position of the remote doping. When the doping was in the silicon layer the mobility was very low (80 $cm^2/V\,s$), while in the other case, where the doping was in the germanium, a high mobility (2000 $cm^2/V\,s$) was found,[6] see Fig. 11.

In Fig. 11 we compare our theoretical results with the experimental findings. Three scattering mechanisms are included. The configuration for the remote doping scattering mechanisms is given in the inset of Fig. 11. As a model for the superlattice structure we used for the remote doping scattering mechanisms three impurity layers with

$$F_R(q,z_i)^2 = \sum_{k=-1}^{1} F_R(q,2ak + z_i)^2 \tag{27}$$

and $n_i = n$. This form factor corresponds to the oscillatory behavior of $\mu_R$ versus the position of the dopant layer. The maximal mobility at $z_i = -30$ Å and the minimal mobility at $z_i = +30$ Å are both determined by the remote doping scattering mechanism. For the dashed line multiple-scattering effects are neglected and only remote scattering is considered [Eqs. (2), (8), and (27)]. The theory cannot describe quantitatively the experimental results. The solid line in Fig. 11 is for the three scattering mechanisms and multiple-scattering effects are included. For the homogeneous background scattering we used $N_B = 10^{17}$ $cm^{-3}$ and then $\mu_B = 6.5 \times 10^4$ $cm^2/V\,s$ for $n = 5 \times 10^{12}$ $cm^{-2}$. For surface-roughness scattering we used $\Delta = 6$ Å, and $\Lambda = 30$ Å and then $\mu_S = 7.6 \times 10^4$ $cm^2/V\,s$ for $n = 5 \times 10^{12}$ $cm^{-2}$. The difference between the solid line and the dashed line for $z_i = -30$ Å is due to these two additional scattering processes. The difference between the two lines at $z_i = 30$ Å is due to the multiple-scattering effects for remote doping.

One could argue that for $z_i = a/2$ there could be a strong band bending due to the impurity layer and the effective width of the quantum well for the remote doping scattering should be smaller than the width of the quantum well. In Fig. 12 we have plotted $\mu_R$ for one impurity layer versus the width of the quantum well and the mobility decreases with decreasing quantum-well thickness. But the effect is too small for an explanation of the discrepancies between theory and experiment, see Fig. 11.

In Fig. 13 we predict the $C(\alpha,n)$ behavior for the configuration as in the inset of Fig. 11 and with the same parameters as in Fig. 11. The solid line is according to Eq. (20c) and demonstrates Eq. (21). But we want to mention that multiple-scattering effects, as discussed in Sec. III D could destroy the linear temperature dependence in samples with low mobility.

A full understanding of the discrepancies between

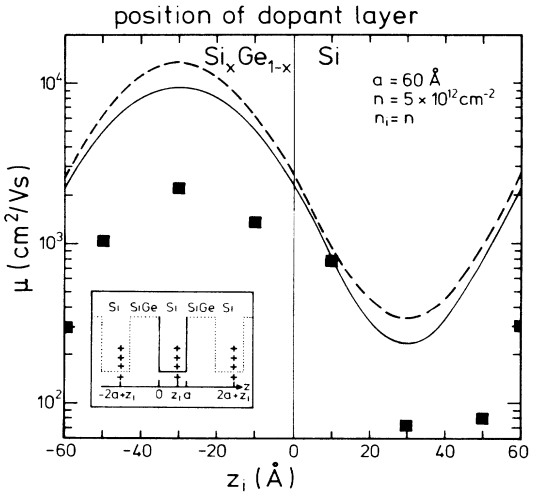


FIG. 11. Mobility versus the position of the dopant layer $z_i$. The dashed line is due to Eqs. (2) and (8) for remote doping. The solid line is the self-consistent theory for the three scattering mechanisms ($\Delta = 6$ Å, $\Lambda = 30$ Å, $N_B = 10^{17}$ $cm^{-3}$). The squares are experimental results from Ref. 6 for $T = 20$ K. The theory is for $T = 0$. The inset shows the configuration of the remote doping layers, see Eq. (27).

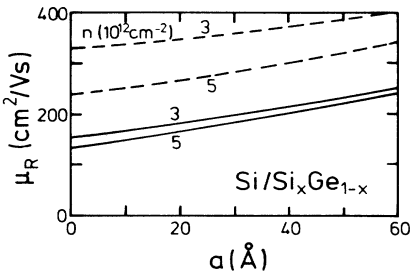


FIG. 12. Mobility versus quantum-well thickness for a single quantum well and remote doping with $n_i = n$ and $z_i = a/2$. For the dashed lines self-consistent effects are neglected while for the solid lines self-consistent effects are included.

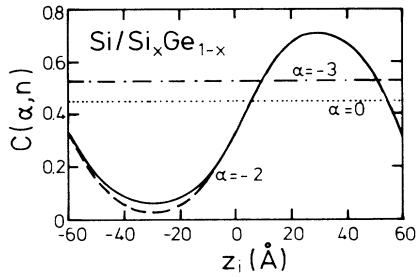


FIG. 13. $C(\alpha,n)$ versus position of the dopant layer. The dotted line is for surface roughness, the dashed line for remote doping, the dashed-dotted line for homogeneous background doping. The solid line is for the three scattering mechanisms according to Eq. (20c). The parameters are the same as in Fig. 11.

theory and experiment in Fig. 11 is not available. A larger $\Delta$ for the surface-roughness scattering would decrease the mobility, and agreement between theory and experiment could be achieved for $-60 < z_i/\text{Å} < 0$. But the necessary value for $\Delta$ is 30 Å, and this value is unrealistic. Another choice of $\Lambda$ would even increase the necessary value for $\Delta$. The mobility at about $z_i \approx 30$ Å would not be changed by such a big surface-roughness scattering.

It seems that the disorder connected with the dopant layer is much higher than in our theoretical model. This is suggested by the following consideration. The ratio between the mobility at $z_i = -30$ Å and $z_i = 30$ Å is about 31 in experiment. Our theory (Fig. 11) gives for this ratio a value of 30.6 (dashed curve). The only way to increase disorder in our model for remote doping is to use $n_i > n$.

### B. Model II: $n_i = 5n$ for remote doping

Figure 14 shows our theoretical results with the experimental results for remote doping $n_i = 5n$ and $F_R(q,z_i)^2$ from Eq. (27). The dashed line describes the experimental results quite well. Due to multiple-scattering effects (solid line) a metal insulator is expected for 16 Å $< z_i <$ 44 Å. The origin for the $n_i = 5n$ behavior could be that in the implantation process also charged impurities are built into the remote doping layer. These impurities only contribute to $n_i$, but not to $n$. It could also be the case that some doubly ionized impurities are built in.

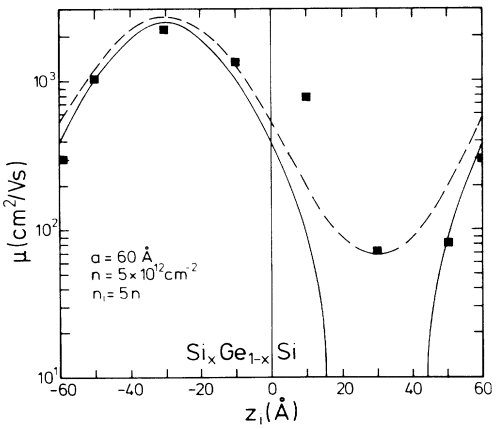


FIG. 14. Mobility versus position of the dopant layer for remote impurity scattering. The solid line is the self-consistent theory and for the dashed line the self-consistent effects are neglected. The squares are experimental results from Ref. 6 for $T = 20$ K. The theory is for $T = 0$.

It has been found in experiment[36] that the electron density depends on $z_i$. For $z_i = 30$ Å an electron density $n \approx 8 \times 10^{12}$ cm$^{-2}$ has been found. In this case the metal-insulator transition would be expected in a much smaller $z_i$ range than for $n = 5 \times 10^{12}$ cm$^{-2}$, but this $z_i$ range again depends on $n_i$. At the moment it seems that our model II describes the experiments of Ref. 6 much better than our model I. But the factor 5 between $n_i$ and $n$ seems to be very high. More experimental results are necessary and the design of the quantum wells for these experiments is discussed in the next section.

## VI. CONCLUSION

In this paper the transport properties of a two-dimensional electron gas confined in a quantum well have been discussed and compared with experiments. With Eq. (1) we have assumed that the barrier height is infinite. In real systems, the barrier height is finite, which leads to a penetration of the wave functions into the range $z > a$ and $z < 0$. In silicon the penetration effects are considerably reduced in comparison to GaAs quantum wells due to the small factor $(m^*/m_z)^2$, see Eq. (4). We believe that the penetration effects are negligible in the case of impurity scattering. Because of the finite barrier height, the effective quantum-well width for the surface-roughness scattering is somehow increased in comparison to $a$. The surface-roughness scattering depends strongly on the quantum-well width and we expect a weaker dependence of the mobility on $a$ if the penetration effects are taken into account.

We have restricted our calculation to one subband. For high electron densities more than one subband is occupied. For $n < 3 \times 10^{12}$ cm$^{-2}$, recent calculations indicate[7] that only one subband is occupied. But for a small occupation of the second subband our theory will describe the correct trend of mobility measurements. So we conclude that our theory should not be applied to densities much higher than $5 \times 10^{12}$ cm$^{-2}$. In other systems the range of applicability of our theory may be even higher.

With decreasing quantum-well width the energy of the ground state of the quantum well shifts to higher energy. For given doping conditions the electron density decreases then with decreasing quantum-well width. By comparing mobility measurements versus quantum-well width with our theory, conclusive results can only be obtained if the actual electron density is determined for every quantum well. We expect that this effect becomes important for $a < 40$ Å.

We made the approximation that both surfaces at the quantum-well boundary are characterized by the same surface-roughness parameters $\Delta$ and $\Lambda$. In the more general case one has to use four parameters and for very thin quantum wells, $a < 2\Delta$, also a correlation between the two surfaces has to be considered. This effect would again in-

crease the number of model parameters.

For $n = 5 \times 10^{12}$ cm$^{-2}$ as in experiment[36] the relevant scattering mechanism which determines the mobility is the remote doping. Surface-roughness scattering and background doping can be neglected for $a > 40$ Å. For $a < 40$ Å surface-roughness scattering becomes very important. The experimental values of the mobility are much lower than predicted from theory with $n_i = n$, and it seems that much more disorder is introduced into the system: $n_i = 5n$. But we expect that samples with $n_i = n$ can also be produced.

It has been shown that in thin quantum wells localization is expected at high electron density due to surface-roughness scattering. This effect could be easily seen in experiment with thin quantum wells, and such experiments would be very helpful to determine the surface-roughness parameters $\Delta$ and $\Lambda$. If the surface roughness limits the mobility (for $a < 40$ Å) in the case where the remote doping is in the germanium layer, then this limit should strongly depend on the thickness of the quantum well. The coefficient $C(0,n)$ also depends on $\Lambda$ and could be used to determine $\Lambda$. The concept of localization due to surface-roughness scattering is new and is a novel aspect of quantum wells. In silicon inversion layers the surface-roughness scattering decreases with decreasing density and $A = 1$ is difficult to achieve there.[37] Furthermore, such quantum wells could verify our concept of localization,[13] in contrast to the results of weak localization.[38]

In thick quantum-well structures, surface-roughness scattering becomes unimportant and the mobility limits in this system are given by our Figs. 4 and 5, at least for small homogeneous background doping. Thick quantum wells have a higher mobility, too, if only remote doping is considered. During the preparation of the remote doping layers by secondary implantation,[8] the density of ionized atoms should be carefully controlled. Then a discrimination between our model I ($n_i = n$) and our model II ($n_i = 5n$) should be possible.

In samples with no, or weak, remote doping outside of the quantum well, a big quantum-well thickness and a high background doping density, the mobility at low density is dominated by the background doping. Then the metal-insulator transition due to this scattering process should be measurable. Also the non-Drude behavior of the conductivity could then be seen in experiment.

In conclusion, we have given the mobility limits in silicon quantum wells due to background doping, remote doping, and surface-roughness scattering. The phase diagram for the metal-insulator transition is predicted. We have suggested some quantum-well structures in order to discriminate the different scattering mechanisms.

## ACKNOWLEDGMENTS

I am grateful to Dr. G. Abstreiter for many discussions and for his suggestion to do this work. This work was supported in part by the Ernst von Siemens Stipendium of the Siemens AG.

[1]T. Ando, A. B. Fowler, and F. Stern, Rev. Mod. Phys. **54**, 437 (1982).
[2]A. C. Gossard, Surf. Sci. **153**, 1153 (1985).
[3]G. Abstreiter, H. Brugger, T. Wolf, H. Jorke, and H. J. Herzog, Phys. Rev. Lett. **54**, 2441 (1985).
[4]R. People, J. C. Bean, B. V. Lang, A. M. Sergent, H. L. Störmer, K. W. Wecht, R. T. Lynch, and K. Baldwin, App. Phys. Lett. **45**, 1231 (1984).
[5]F. Cerdeira, A. Pinczuk, J. C. Bean, B. Battlogg, and B. A. Wilson, App. Phys. Lett. **45**, 1138 (1984).
[6]G. Abstreiter, H. Brugger, T. Wolf, R. Zachai, and Ch. Zeller, in *Two-Dimensional Systems: Physics and New Devices*, edited by G. Bauer, F. Kuchar, and H. Heinrich (Springer, Berlin, 1986), p. 130.
[7]Ch. Zeller and G. Abstreiter, Z. Phys. B **64**, 137 (1986).
[8]H. Jorke and H. Kibbel, in *Proceedings of the 1st International Si-MBE Symposium, May 1985, Toronto*, edited by J. C. Bean (Electrochemical Society, Pennington, 1985), p. 352.
[9]S. Mori and T. Ando, J. Phys. Soc. Jpn. **48**, 865 (1980).
[10]J. Lee, H. Spector, and V. Arora, Appl. Phys. Lett. **42**, 363 (1983); J. Appl. Phys. **54**, 6995 (1983), and references cited therein.
[11]H. Spector and V. Arora, Surf. Sci. **159**, 425 (1985).
[12]F. Stern and W. Howard, Phys. Rev. **163**, 816 (1967).
[13]A. Gold and W. Götze, Solid State Commun. **47**, 627 (1983); Phys. Rev. B **33**, 2495 (1986).
[14]A. Gold, Phys. Rev. Lett. **54**, 1079 (1985); Phys. Rev. B **32**, 4014 (1985).
[15]A. Gold and V. T. Dolgopolov, Phys. Rev. B **33**, 1076 (1986).
[16]R. E. Prange and T. W. Nee, Phys. Rev. **168**, 779 (1968).
[17]F. Stern, Phys. Rev. Lett. **18**, 546 (1967).
[18]M. Jonson, J. Phys. C **9**, 3055 (1976).
[19]W. Götze and P. Wölfle, Phys. Rev. B **6**, 1226 (1972).
[20]N. Tzoar, P. N. Platzman, and A. Simons, Phys. Rev. Lett. **36**, 1200 (1976).
[21]X. L. Lei and J. Q. Zhang, J. Phys. C **19**, L73 (1986).
[22]A. Gold and W. Götze, Solid State Electron. **28**, 87 (1985).
[23]A. Gold, W. Götze, C. Mazuré, and F. Koch, Solid State Commun. **49**, 1085 (1984).
[24]F. Koch and A. Gold, Surf. Sci. **170**, 370 (1986).
[25]F. Stern, Phys. Rev. Lett. **44**, 1469 (1980).
[26]K. M. Cham and R. G. Wheeler, Phys. Rev. Lett. **44**, 1472 (1980).
[27]S. I. Dorozhkin and V. T. Dolgopolov, Pis'ma Zh. Eksp. Teor. Fiz. **40**, 245 (1984) [JETP Lett. **40**, 1019 (1985)].
[28]J. L. Smith and P. J. Stiles, Solid State Commun. **58**, 511 (1986).
[29]C. Mazuré and F. Koch (unpublished).
[30]W. Götze, Solid State Commun. **27**, 1393 (1978).
[31]A. Gold, Z. Phys. B **63**, 1 (1986).
[32]D. Olego, A. Pinczuk, A. C. Gossard, and W. Wiegmann, Phys. Rev. B **25**, 7867 (1982).
[33]E. Batke, D. Heitmann, J. P. Kotthaus, and K. Ploog, Phys. Rev. Lett. **54**, 2367 (1985).
[34]S. J. Allen, D. C. Tsui, and R. A. Logan, Phys. Rev. Lett. **38**, 980 (1977).
[35]D. Heitmann, Surf. Sci. **170**, 332 (1986).
[36]T. Wolf, Diplomarbeit, Technische Universität München, 1985.
[37]A. Gold, Solid State Commun. **60**, 531 (1986).
[38]E. Abrahams, P. W. Anderson, D. C. Licciardello, and T. V. Ramakrishnan, Phys. Rev. Lett. **42**, 673 (1979).